processes

MDPI

Article

Visible Fenton Degradation of Bisphenol A by Boron-Doped, Graphene-Oxide-Coated Nano-Fe_3O_4

Boxia Liu [1], Xiayan Zhang [2] and Zhi Song [2,*]

[1] School of Biological Science and Engineering, North Minzu University, Yinchuan 750021, China
[2] Chemical Science and Engineering College, North Minzu University, Yinchuan 750021, China
* Correspondence: 2021733@nmu.edu.cn

Abstract: Phenolic pollutants in industrial wastewater are considered to be harmful aromatic compounds. With the development of industry and pharmaceuticals, phenolic pollutants and their derivatives have gradually started to affect people's daily lives. Therefore, it is necessary to strictly control the content of phenolic pollutants in industrial wastewater, not only for the natural environment but also for human life. The research optimized the existing treatment methods for classified pollutants, and successfully prepared a heterogeneous photo-Fenton catalyst Fe_3O_4@B-rGO (9.3%). The characterization results of the catalyst showed that the synthesis of the catalyst was successful, and its specific surface area was 11.28 (m^2/g), and the pore volume area was 0.137 (m^3/g), respectively, which were larger than those of the other two comparative catalysts. In addition, the research conclusion also showed that the catalyst prepared during the research had good catalytic activity, the treatment efficiency of Fe_3O_4@B-rGO (9.3%) to bisphenol A could reach 100%, and the mineralization rate could reach 67.4%. In the reaction, the main active radicals are generated, and catalyst Fe_3O_4@B-rGO (9.3%) can produce more active free radicals compared with Fe_3O_4 and Fe_3O_4@rGO.

Keywords: visible light; heterogeneous; degradation; phenols; Fe_3O_4@B-rGO; catalyst

Citation: Liu, B.; Zhang, X.; Song, Z. Visible Fenton Degradation of Bisphenol A by Boron-Doped, Graphene-Oxide-Coated Nano-Fe_3O_4. *Processes* **2022**, *10*, 2582. https://doi.org/10.3390/pr10122582

Academic Editors: Jacek Gebicki, Pawel Sobieszuk and Piotr Rybarczyk

Received: 26 October 2022
Accepted: 26 November 2022
Published: 3 December 2022

1. Introduction

With the deepening of the world's industrialization process, humanity's demand for resources and energy is also increasing [1]. From the perspective of the current development model of human society, there is a huge waste of resources and energy. Such development is undoubtedly achieved through sacrifice [2]. Water pollution, the energy crisis and other issues have also received critical attention. Among them, the problem of water pollution is the top priority in terms of environmental pollution, and the development of effective sewage treatment technology has always been the focus of environmental protection work [3]. The treatment of industrial wastewater has to be considered in water pollution control. Industrial wastewater not only causes harm to the ecological environment, but also negatively affects human health. On the one hand, it affects the survival of animals and plants. On the other hand, when people use polluted water in their lives, the health of the surface water will be threatened [4,5]. Compounds are widely used in various industrial branches, including the petrochemical industry, coal processing and metallurgical casting [6]. These phenolic compounds enter the natural ecosystem via the discharge of municipal sewage or industrial wastewater from production activities in chemical, gasoline, tincture, and pharmaceutical industries [7]. Moreover, with the increasing demand for phenolic compounds at home and abroad, the investment, construction and production of phenolic compound production equipment is also increasing year by year, which also means an increase in the discharge of phenol-containing wastewater, which means that developing a more efficient wastewater treatment technology is crucial [8]. Therefore, this research focuses on the optimization of treatment technology for phenol-containing wastewater. The main research focuses on the mechanism of heterogeneous photo-Fenton

treatment of bisphenol A pollutants with boron-atom-doped, graphene-oxide-wrapped nano-iron tetroxide.

2. Related Work

Given the importance of industrial wastewater treatment to ecosystems as well as human health, many researchers have conducted extensive research in this context [9,10]. Qian et al. proposed a heterogeneous Fenton catalyst driven by visible light. The research conclusions showed that the heterogeneous photo-Fenton process in this system enhances the efficiency of HO· generation and Fe(III)/Fe(II) transition, further activating the interfacial catalytic sites. Extremely high treatment and mineralization efficiencies were achieved [11]. Garcia-Muñoz et al. [12] paid attention to the reuse of catalysts and photo catalysts in water treatment. On this basis, they developed a single–dual catalyst strategy. The results of the study showed that the stability of the catalyst was more than doubled, and its reaction rate was also significantly improved, and the catalyst could completely mineralize the pollutants in the combined advanced oxidation process at neutral pH. Zhu et al. [13] adopted a new approach to solve the reaction rate problem in the heterogeneous Fenton reaction, namely the formation of Fe(II) from Fe(III) under the condition of consuming a large amount of hydrogen peroxide. The research conclusion showed that the reaction system exhibits efficient performance in the photo-Fenton reaction. Phan et al. studied the catalysis of metalions in Fenton reaction, and selected copper as doping ion. Compared with lanthanum ferrite without copper atoms, the new catalyst could degrade organic pollutants more efficiently. Based on the photo-Fenton treatment principle, the researchers optimized its application judging from the specific amount of hydrogen peroxide and catalyst, and the pH value of the solution. The results showed that the catalyst had strong stability and could be reused [14]. Chen et al. [15] prepared a new CoII-Fenton-based heterogeneous catalyst, which can degrade organic dyes and antibiotics under photo catalysis. It can be used in the range of 3–9 pH-responsive environments. The results also showed that such catalysts can be recovered and reused.

Kilic et al. [16] paid attention to the use of an advanced oxidation process in the treatment of phenolic pollutants. They introduced sulfur atoms into the reaction system to catalyze the treatment of phenolic substances. The results showed a better treatment effect. Guo et al. [17] put forward a method of solvent selection which was based on structural feature integration computer-aided molecular design. In this study, allyl ether was selected as an effective solvent for the removal of hydroquinone. The extraction efficiency of commonly used solvents for methyl propyl ketone was compared, and a new method for methyl propyl ketone to recover phenols was developed. Liu et al. [18] synthesized a heterogeneous light Fenton catalyst by heating borane mixture. The results showed that the addition of a boron atom caused the catalyst to exhibit excellent Fenton's performance, and the catalyst had strong stability and magnetic separation performance. Among them, @B-rGO with an Fe_3O_4-doped boron concentration of 9.3% had better catalytic performance than other comparative catalysts, which could accelerate the oxidation-reduction between divalent Fe ions and trivalent Fe ions. Starting from the direction of electro-oxidation process, Abou-Taleb et al. [19] studied a new method to remove phenol from petroleum wastewater. The conclusion of the study showed that the method could completely remove phenol from the initial concentration solution of about 6.8 mg/L if the optimal reaction conditions could be provided. In addition, considering the oxygen demand, the method could remove 50–60% of the organic matter. This method is more economical than traditional methods. Kadhum et al. [20] used nano-zero-valent iron and silty clay-supported nano-zero-valent iron as the third electrode in the electrochemical reaction, and the cathode and anode of the battery were both aluminum plates, thus forming an electrochemical cell to remove aqueous phenol. The results showed that the first way electrochemical process had a fairly high efficiency in treating phenol-containing wastewater. The removal rate of phenol by the two electrochemical techniques could reach 96.1% and 97.8%, respectively.

To sum up, in the past studies, there have been many relatively mature studies on heterogeneous photo-Fenton reaction and chemical treatment methods of phenolic pollutants, including doping boron atoms in catalysts, but there is still room for improvement in related studies. Therefore, this study started from heterogeneous photo-Fenton reaction with boron atoms, trying to prepare catalysts with better catalytic performance and provide better treatment methods for phenolic pollutants.

3. Materials and Methods

The research consists of three parts, the first is the preparation and characterization of the catalyst, the second is the influencing factors and catalytic activity of Fe_3O_4@B-rGO as a catalyst for the treatment of bisphenol A by heterogeneous photo-Fenton, and the last is Fe_3O_4@B-rGO mechanism of heterogeneous photo-Fenton treatment of Bisphenol A.

3.1. Preparation and Characterization of Catalysts

In this experiment, the preparation process of the catalyst is included, and the experimental equipment used is shown in Table 1.

Table 1. Instruments of the experiments.

Laboratory Apparatus	Instrument Model	Manufacturer
Electronic balance	AY220	Shimadzu Corporation of Japan
Digital single channel pipetting gun	SDCA-704178	Germany BRAND company
Centrifuge	TGL-16A	Hu'nan pingfan Technology Co., Ltd.
Heating constant temperature magnetic stirrer	HWCL-1	Zhengzhou Great Wall Instrument Co., Ltd.
Ultrasonic cleaner	HJ69-700B	Beijing xihuayi Technology Co., Ltd.
Micro peristaltic pump	BQ50S	Baoding Leifu Fluid Technology Co., Ltd.
Mechanical stirrer	SRH15/RW20	Beijing zhongxi yuanda Technology Co., Ltd.
Oil bath pot	HH-1/HH-S	Beijing maikeyi Technology Co., Ltd.
Constant temperature blast drying oven	XMTD-8222	Zhejiang Huangyan Tianlong Vacuum Pump Factory
X-ray polycrystalline powder diffractometer	D/MAX-2500/PC	Japan Neo-Confucianism Corporation
Raman spectrometer	Lab RAM HR800	Hoyba Jobbin Yvonne, France
Scanning electron microscope	Merlin compact	Hoyba Jobbin Yvonne, France
Transmission electron microscope	FEP Tecnai G2 F30	FEI Company of America
Transmission electron microscope with spherical aberration correction	Titan G260-300	Japanese calendar high-tech enterprises
X-ray photoelectron spectrometer	PHI Quantera II	UIVAC corporation of Japan
Specific surface and void analyzer	TRISTAR II3020	Mike instruments Inc.

The main chemical reagents used in this experiment are shown in Table 2.

Table 2. Chemical reagents of the experiments.

Drug Name	Chemical Formula	Manufacturer
Phosphoric acid	Analytically pure H_3PO_4	Tianjin Hengxing Chemical Reagent Manufacturing Co., Ltd.
Sulfuric acid	Analytically pure H_2SO_4	Chengdu kelong Chemicals Co., Ltd.
Graphite powder	C	Tianjin Damao Chemical Reagent Factory
Potassium permanganate	Analytically pure $KMnO_4$	Tianjin kemiou Chemical Reagent Co., Ltd.
Hydrogen peroxide	hydrogen peroxide	Shanghai National Medicine Group Chemical Reagent Company
Nanometer ferroferric oxide	Analytically pure Fe_3O_4	Tianjin kemiou Chemical Reagent Co., Ltd.
Aminopropyltriethoxysilane	Analytically pure $NH_2(CH_2)_3Si(OC_2H_5)_3$	Shanghai McLean Biochemical Technology Co., Ltd.
Borane tetrahydrofuran complex	Analytically pure $C_4H_{11}BO$	Shanghai McLean Biochemical Technology Co., Ltd.

The preparation of the catalyst needs three stages, namely the preparation of graphene oxide (GO), Fe_3O_4@rGO and Fe_3O_4@B-rGO.The first is the preparation of graphene oxide (GO), and the modified Hummers method is used to prepare GO, its specific preparation process is shown in Figure 1.

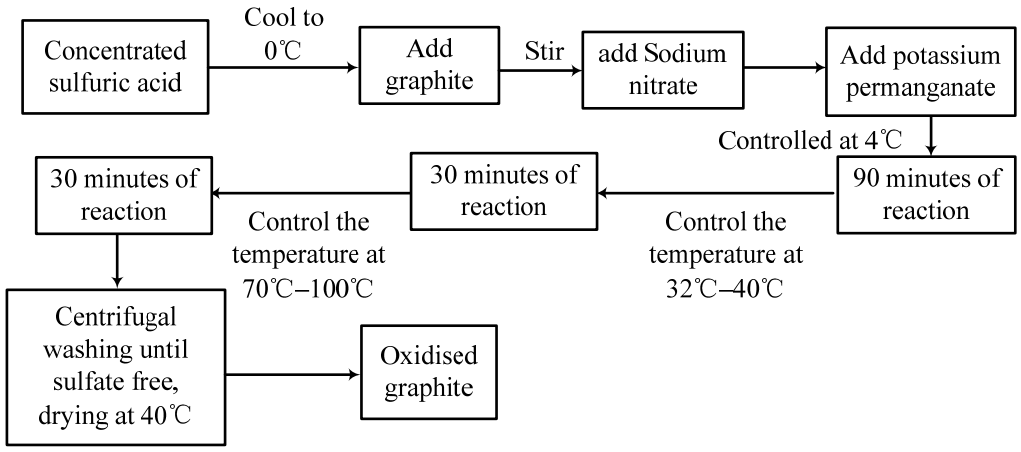

Figure 1. Graphite oxide preparation process technology roadmap.

After GO is obtained by the method shown in Figure 1, the experiment progresses to the second step. In this step, the hydrothermal method is used to reduce GO to rGO, and the catalyst Fe_3O_4@rGOis prepared. The final step is the preparation of Fe_3O_4@B-rGO, which is similar to that of Fe_3O_4@GO, by adding different concentrations of borane tetrahydrofuran to the Fe_3O_4@rGO solution before oil bath heating. The solution can obtain Fe_3O_4@B-rGO catalysts doped with different concentrations of boron atoms. The research explores the preparation methods of Fe_3O_4@B-rGO, Fe_3O_4@rGO and Fe_3O_4 doped with different boron atom concentrations, and a total of four concentrations of Fe_3O_4@B-rGO solutions are prepared, in which the mass concentrations of doped boron atoms are 4.6%, 6.8%, 9.3% and 12.5%, respectively. The analysis results show that Fe_3O_4@B-rGO (9.3%) has the best catalytic effect.

Characterization of the catalysts includes Raman spectroscopy analysis, X-ray diffraction analysis, transmission electron microscopy analysis and scanning electron microscopy, X-ray photoelectron spectroscopy analysis, nitrogen adsorption–desorption curve analysis,

and spherical aberration corrected transmission electron microscopy analysis. The crystal structure of the catalyst is analyzed by X-ray polycrystalline powder diffractometer, and the test results are analyzed by Jade.5.0 software developed by MDI Company in California, USA. The instrument selected in the Raman spectroscopic analysis is the French Horiba Jobin Yvon Lab RAM HR800 Micro Confocal Raman Spectrometer. The selected electron microscope model is Zeiss Merlin compact, and the transmission electron microscope model is Tecnai G2 F30 FET. The purpose of X-ray photoelectron spectroscopy analysis is to detect the elemental composition and chemical valence state of the sample surface. The model of the instrument selected is PHI Quantera II. The instrument selected for the spherical aberration correction transmission electron microscope analysis is Titan G260-300, and the purpose of this process is to analyze the chemical structure and element distribution of the sample.

3.2. Study on Influencing Factors and Catalytic Activity of Heterogeneous Photo-Fenton Treatment of Bisphenol A Using Fe_3O_4@B-rGO as Catalyst

The oxidation method using iron salt to activate hydrogen peroxide (H_2O_2) is called Fenton reagent. Hydrogen peroxide oxidation alone is ineffective for high concentrations of some refractory pollutants, while transition metal salts, ozone and ultraviolet light can activate hydrogen peroxide to form hydroxyl groups as strong oxidants. The specific chemical reaction process is shown in Equations (1)–(3).

$$O_3 + H_2O_2 \rightarrow \cdot OH + O_2 + HO_2{}^- \quad (1)$$

$$Fe^{2+} + H_2O_2 \rightarrow Fe^{3+} + \cdot OH + OH^- \quad (2)$$

$$H_2O_2 + UV \rightarrow 2 \cdot OH \quad (3)$$

Equation (1) represents the reaction process of hydrogen peroxide and ozone, Equation (2) represents the reaction process of iron salt and hydrogen peroxide. Equation (3) is the reaction process of ultraviolet rays and hydrogen peroxide.

A large amount of iron salts is used in the traditional homogeneous Fenton technology treatment process, which makes it difficult to recover the iron ions in the solvent, and the iron sludge produced by the reaction will also cause serious pollution to the environment. Switching to solids can avoid these problems well, and such a technique is known as the heterogeneous Fenton technique. The basic principle of the heterogeneous Fenton reaction is shown in Equations (4)–(6).

$$Fe^{3+} + H_2O_2 \rightarrow Fe^{3+}H_2O_2 \quad (4)$$

$$Fe^{3+}H_2O_2 \rightarrow Fe^{2+} + HO_2{}^- + H^+ \quad (5)$$

$$Fe^{2+} + H_2O_2 \rightarrow Fe^{3+} + \cdot OH + OH^- \quad (6)$$

In the above process, Fenton's reagent is a catalytic oxidation mixture including ferrous ion and hydrogen peroxide, and the reaction can undergo a strong chemical reaction and generate non-selective hydroxyl radicals.

$$H_2O_2 + hv \rightarrow 2OH^- \quad (7)$$

$$\cdot OH + HO_2{}^- \rightarrow HO_2 \cdot + OH^- \quad (8)$$

$$HO_2 \cdot + H_2O_2 \rightarrow HO_2 + \cdot OH + O_2 \quad (9)$$

$$\cdot OH + H_2O_2 \rightarrow O_2 \cdot{}^- + H_2O \quad (10)$$

Equations (7)–(10) describe radical chain reactions initiated and propagated by hydroxyl radicals, and light is used as a catalytic condition during this process.

$$O_2 \cdot{}^- + H^+ \rightarrow HO_2 \cdot \quad (11)$$

$$Fe^{3+} + H_2O + hv \rightarrow Fe^{2+} + \cdot OH + H^+ \quad (12)$$

$$\cdot OH + \text{phenol} \rightarrow \text{products} \quad (13)$$

Equations (11)–(13) are the oxidation process of organic substances and reducing substances, wherein Equation (13) describes the treatment process of phenolic compounds by hydroxyl radicals. In the Fenton reaction, the catalytic efficiency is determined by the amount and ratio of Fe^{2+}/Fe^{3+}. In the presence of hydrogen peroxide, any substance that can generate Fe^{2+} or Fe^{3+} can undergo Fenton reaction to degrade organic matter.

In addition, the study takes bisphenol A as a typical phenolic pollutant sample, and selects the catalyst Fe_3O_4@B-rGO as the research object to study the factors affecting its treatment of bisphenol A and test its catalytic activity and stability. All the reaction experiments in the research are carried out under the catalysis of visible light, and the photoreactor with a xenon lamp as the simulated light source is chosen as the experimental environment.

The study uses high-performance liquid chromatography to test the concentration of bisphenol A. The sample amount used in a single measurement is 20 μL. The residence time and peak time of the sample are 6.5 min and 4.2 min, respectively. A total of 8 bisphenol A solutions of different concentrations are prepared in the study, and the concentration of bisphenol A in these solutions is kept between 1 and 100 mg/L. Different concentrations of bisphenol A solutions would correspond to different peak areas in the detection. In the drawing of the standard curve of bisphenol A, the concentration of bisphenol A is taken as the abscissa and the peak area as the ordinate. The drawn curve is shown in Figure 2.

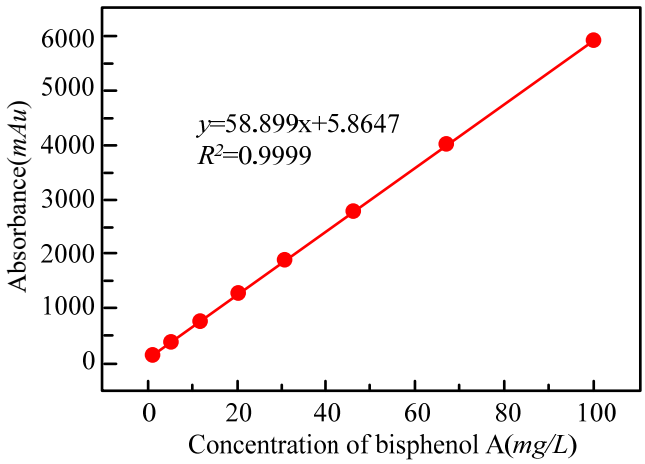

Figure 2. The standard curve of bisphenol A concentration.

As shown in Figure 2, the fitting degree of the standard curve is 0.9999, so the standard curve can be used to measure the concentration of bisphenol A in the sample. The calculation method of the treatment rate of bisphenol A is shown in Equation (14).

$$D(\%) = \frac{C_0 - C_t}{C_0} \times 100\% \quad (14)$$

wherein C_0 is the initial reaction concentration of bisphenol A, C_t is the concentration of bisphenol A at time t of reaction, where t is the photocatalytic reaction time. In the determination of solution TOC, samples are taken every 20 min, and then samples are filtered with a 0.45 μm filter and analyzed by a total organic carbon analyzer. The mineralization rate of bisphenol A can be obtained from Equation (15).

$$M(\%) = \frac{TOC_0 - TOC_t}{TOC_0} \times 100\% \quad (15)$$

TOC_0 is the TOC value of the reaction of bisphenol A, and TOC_t is the TOC value of bisphenol A at time t of reaction.

3.3. Mechanism of Fe_3O_4@B-rGO Heterogeneous Photo-Fenton Treatment of Bisphenol A

In this study, the mechanism of heterogeneous photo-Fenton treatment of bisphenol A pollutants with Fe_3O_4@B-rGO as catalyst is discussed. The process includes free radical trapping test, electron spin resonance test, UV-Vis diffuse reflectance test, electrochemical test, electron density of state calculation, Fe^{2+} production and hydrogen peroxide consumption test.

In the free radical trapping test, the study uses isopropanol, p-benzoquinone and ethylenediaminetetraacetic acid as trapping agents to trap the three kinds of free radicals, namely ·OH, $O_2\cdot^-$ and h^+, respectively. Taking the isopropanol-hydrogen peroxide-air system as an example, the reaction equation is shown in Equation (16).

$$2HCHO + OH^- \rightarrow HCOO^- + CH_3O^- \quad (16)$$

The specific operation is to add different concentrations of capture agents to the system, take samples within a fixed time, and measure the concentration of bisphenol A. According to the influence of different inhibitors on the treatment of bisphenol A, the free radicals that play a major role in the treatment of bisphenol A by the catalyst Fe_3O_4@B-rGO are deduced.

As the adduct of ·OH and $O_2\cdot^-$,water and methanol are used as the reaction solvents of ·OH and $O_2\cdot^-$, respectively, then the adduct is mixed with the reaction solvent at the ratio of 1:1, and finally the free radicals in the reaction system are detected by ESR. The amount of free radicals in the reaction system can be judged by the strength of the detected signal. The stronger the detection signal, the more free radicals are generated in the system.

The UV-Vis diffuse reflectance spectrum of the sample can be measured with a UV-Vis spectrophotometer. The sample is dried and sieved, and $BaSO_4$ is used as a reference to calculate the forbidden band width of the catalyst according to Equation (17).

$$(\alpha hv)^{1/n} = A(hv - Eg) \quad (17)$$

Among them α, h, v, n and A are the light absorption rate, Planck's constant, the frequency of light, the properties of the semiconductor electron transition and a constant, respectively.

Electrochemical tests used in the study include Mott-Schottky test, electrochemical impedance spectroscopy, cyclic voltammetry and transient photocurrent response tests. Specifically, the transparent conductive glass doped with fluorine SnO_2 is the working electrode, the platinum sheet is the counter electrode, the standard calomel electrode is the reference electrode, and Na_2SO_4 is the electrolyte for the reaction.

In the process of calculating the electronic density of states of the reaction system, the study uses the Perdew–Burke–Ernzerhof functional to describe the spin polarization of the electronic structure. The generalized gradient approximation +U method is used to remove the effect of electronic correlation. All calculations are performed in the k-point grid of the Monkhorst-Pack. The specific steps to build the model are as follows. A supercell model is built with 24 iron atoms, 32 oxygen atoms in Fe_3O_4, 50 carbon atoms in rGO, and every 10 atoms in Fe_3O_4@B-rGO (9.3%) A carbon atom corresponds to 1 boron atom.

For the test of Fe^{2+} production and hydrogen peroxide consumption, 8 photoreaction tubes are prepared, representing 8 different reaction times. The catalyst after photoreaction is collected at regular intervals, and added into the colorimetric tube after filtering. Then, add Na_2CO_3, HCl, NH_4F, o-phenanthroline and CH_3COONH_4-CH_3COOH buffer (pH = 4.2) solution to the colorimetric tube, respectively, after dilution, wait for color development, and finally in the ultraviolet visible concentrations are measured in a spectrophotometer. The specific operation steps for measuring the consumption of hydrogen peroxide are as follows. First, add the 2,9-dimethyl-1,10-phenanthroline (DMP) reagent

to the CH_3CH_2OH solution, and prepare a phosphate buffer composed of KH_2PO_4 and K_2HPO_4 (The pH value is about 7). Add the above solutions to the volumetric flask, respectively, shake the volumetric flask until a light yellow substance appears in the liquid in the flask, which is $Cu(DMP)^{2+}$, and finally the concentration of $Cu(DMP)^{2+}$ is measured.

4. Analysis of Results

The analysis of the results includes the characterization analysis of the catalyst and the discussion of the characterization analysis results for the treatment of bisphenol A under different light conditions.

During the characterization and analysis of catalysts, X-ray diffraction analysis is used to analyze the crystal structures of Fe_3O_4@B-rGO, Fe_3O_4@rGO and Fe_3O_4 (9.3%), and the analysis results are shown in Figure 3.

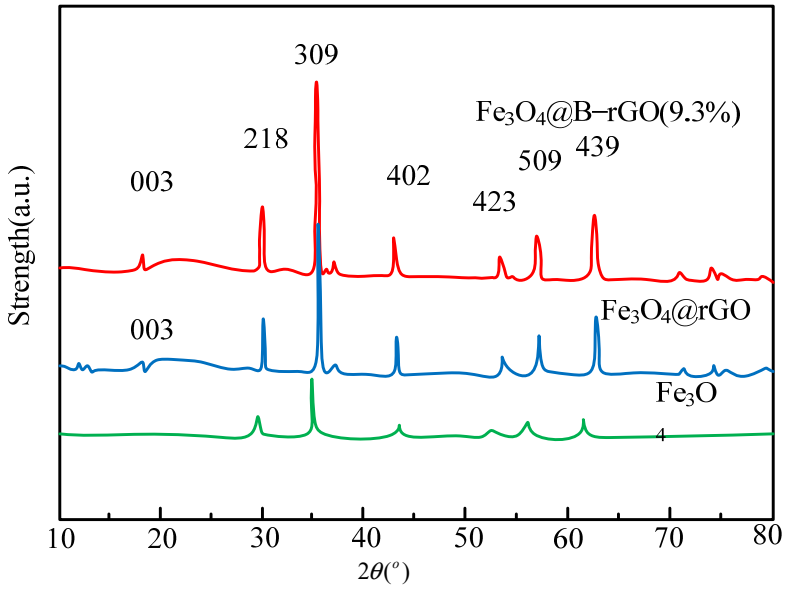

Figure 3. XRD patterns of Fe_3O_4@B-rGO (9.3%), Fe_3O_4@rGO and Fe_3O_4.

As shown in Figure 3, graphene is successfully combined with Fe_3O_4 in Fe_3O_4@rGO and Fe_3O_4@B-rGO (9.3%). However, in the spectra of Fe_3O_4@rGO and Fe_3O_4@B-rGO (9.3%), it can be seen that its characteristic peak has nothing to do with whether boron atoms are doped or not, which is because boron atoms and carbon atoms radii are similar. Raman spectroscopic analysis is used to prove the existence of graphene in the catalysts Fe_3O_4@rGO and Fe_3O_4@B-rGO (9.3%), and judge the defect state density of the catalysts. The analysis results are shown in Figure 4.

As shown in Figure 4, in the catalyst Fe_3O_4@rGO, ID/IG = 0.98, while in the catalyst Fe_3O_4@B-rGO (9.3%), defect density ID/IG = 0.85. Therefore, after doping with boron atoms, the density of defect states of the catalyst is reduced, which is conducive to the generation and migration of photo-generated carriers. To explore the change in the surface morphology of Fe_3O_4 before and after wrapping graphene, SEM and TEM are used to analyze the mixed solutions. The results show that even if boron atoms are doped in the catalyst, its surface topography will not change, this result is similar to the reference results. Investigating the structure of chemical bonds between elements in catalysts using X-ray photoelectron spectroscopy, and the three catalysts Fe_3O_4@B-rGO, Fe_3O_4@rGO and Fe_3O_4(9.3%) were investigated. The results are shown in Figure 5.

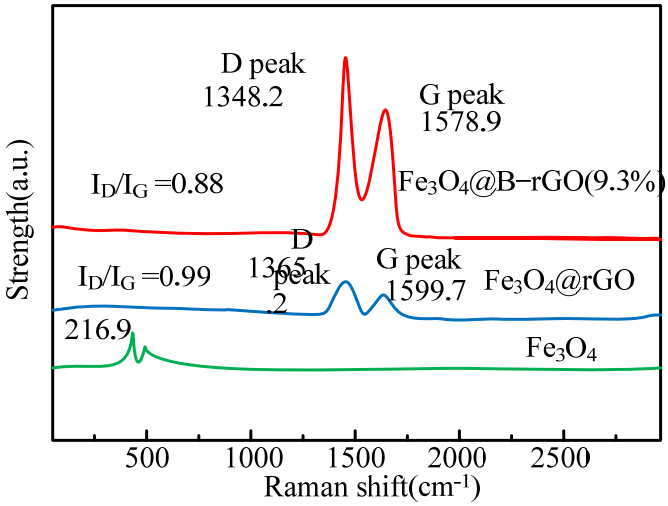

Figure 4. Raman spectra of Fe_3O_4@B-rGO (9.3%), Fe_3O_4@rGO and Fe_3O_4.

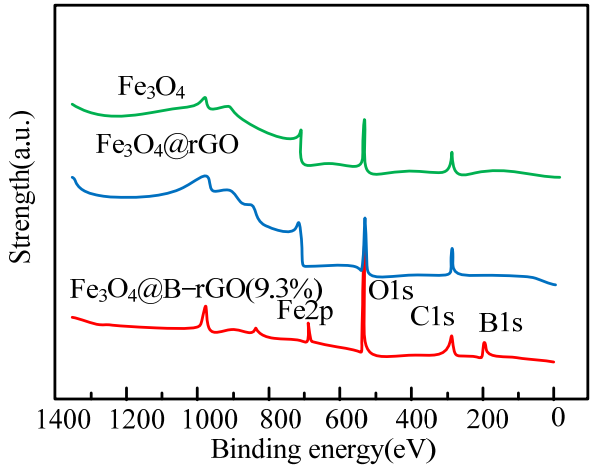

Figure 5. Full XPS spectra of Fe_3O_4@B-rGO (9.3%), Fe_3O_4@rGO and Fe_3O_4.

The boron atoms in the catalyst Fe_3O_4@B-rGO (9.3%) can form CB bonds with the carbon atoms in graphene, which indicates that the boron atoms have been successfully combined with graphene in a chemical bond manner. Spherical aberration-corrected transmission electron microscopy analysis is used to observe the distribution of each element on the catalyst. The analysis results of electron energy loss spectra show that carbon and boron elements are uniformly distributed around Fe_3O_4 and form a core–shell structure. Carbon and boron elements are basically distributed in the same area. It can be seen that the boron element has been uniformly distributed on the graphene structure, and the electron energy loss spectrum analysis of Fe_3O_4@B-rGO (9.3%) shows that it is in the graphene structure. Some carbon atoms are successfully replaced by boron atoms. The specific surface area and pore volume of the catalyst can be calculated using nitrogen adsorption–desorption curve analysis, and the analysis results are shown in Table 3.

Table 3. The properties of Fe_3O_4@B-rGO (9.3%), Fe_3O_4@rGO and Fe_3O_4.

Catalyst	Specific Surface Area (m^2/g)	Pore Volume (m^3/g)	Ms (emu/g)
Fe_3O_4	10.08	0.038	75.4
Fe_3O_4@rGO	42.82	0.182	35.8
Fe_3O_4@B-rGO (9.3%)	43.03	0.141	57.6

From the data shown in Table 3, it can be seen that in terms of specific surface area, Fe_3O_4@B-rGO (9.3%) is 43.03 m^2/g, while Fe_3O_4@rGO is 42.82 m^2/g, the difference between the two is not significant. However, it is significantly higher than the specific surface area of Fe_3O_4 of 11.28 (m^2/g). Moreover, the pore volumes of Fe_3O_4, Fe_3O_4@rGO and Fe_3O_4@B-rGO (9.3%) are 0.037, 0.182 and 0.141 (m^3/g), after the introduction of rGO or B-rGO, for Fe_3O_4, its specific surface area and pore volume are increased, and these properties can cause the pollutants to make full-contact with the active sites of the catalyst, thereby effectively degrading the pollutants. Compared with references, the catalyst prepared in this experiment has a larger specific surface area and pore volume, which can effectively increase the reaction area and reaction speed.

The influence of different illumination conditions on the heterogeneous Fenton system is studied. The research results on the treatment efficiency of bisphenol A are shown in Figure 6. The light intensity is 250 W, 300 W, 400 W, and 500 W, respectively.

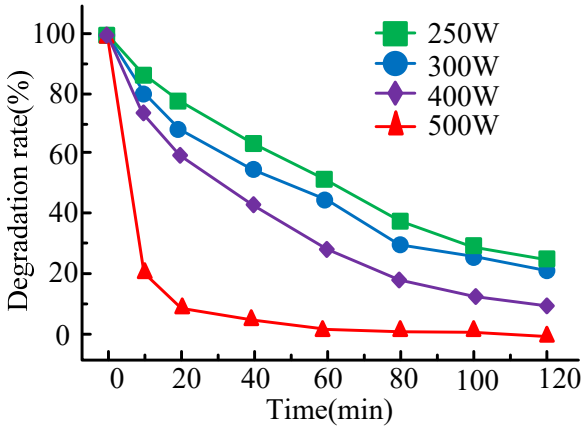

Figure 6. Treatment rate diagram of bisphenol A under different light intensities.

It can be seen from Figure 6 that when the light intensity is 250 W, 300 W, 400 W and 500 W, the corresponding bisphenol A treatment rates at 120 min are 76.4%, 77.9%, 88.4% and 100%, respectively, and the corresponding reaction rate constants are 0.012 min^{-1}, 0.014 min^{-1}, 0.018 min^{-1} and 0.051 min^{-1}, respectively. It can be obtained that when the light intensity increases, the treatment rate of bisphenol A also shows an upward trend, and when the light intensity is 500 W, the treatment efficiency and reaction rate constant of the reaction system to bisphenol A both reach the highest values. To observe and compare the catalytic activity of different catalysts, hydrogen peroxide, hydrogen peroxide/Fe_3O_4@rGO, hydrogen peroxide/Fe_3O_4 and hydrogen peroxide/Fe_3O_4@B-, four different reaction systems of rGO (9.3%) are used to test its treatment effect on bisphenol A. Figure 6 shows the treatment and mineralization of BPA in the reaction system by each catalyst under different conditions.

As shown in Figure 7, in the heterogeneous photo-Fenton system, the treatment efficiency and mineralization efficiency of bisphenol A are both high, which indicates that the heterogeneous photo-Fenton system will generate active species with strong oxidizing properties, thus Bisphenol A is effectively degraded. Furthermore, the results show that the treatment efficiency, mineralization efficiency and reaction rate constant of bisphenol A by Fe_3O_4@B-rGO composites are higher than those of Fe_3O_4 and Fe 3. The values of Fe_3O_4@rGO for these two catalysts are 100% and 67.4%, respectively. Compared with the references, the catalyst in this study can achieve a faster reaction rate, which shows that the performance of the catalyst prepared in this study is better than that of the similar optimizers in the references. In addition, the active radical trapping experiment of the catalyst Fe_3O_4@B-rGO (9.3%) for the treatment of bisphenol A is analyzed, and the results are shown in Figure 8.

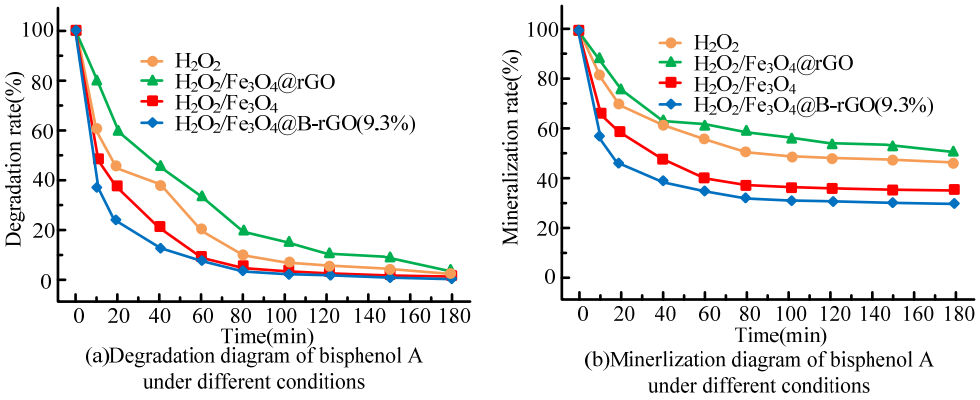

Figure 7. Treatment diagram (**a**) and mineralization diagram (**b**) of bisphenol A by each catalyst under different conditions.

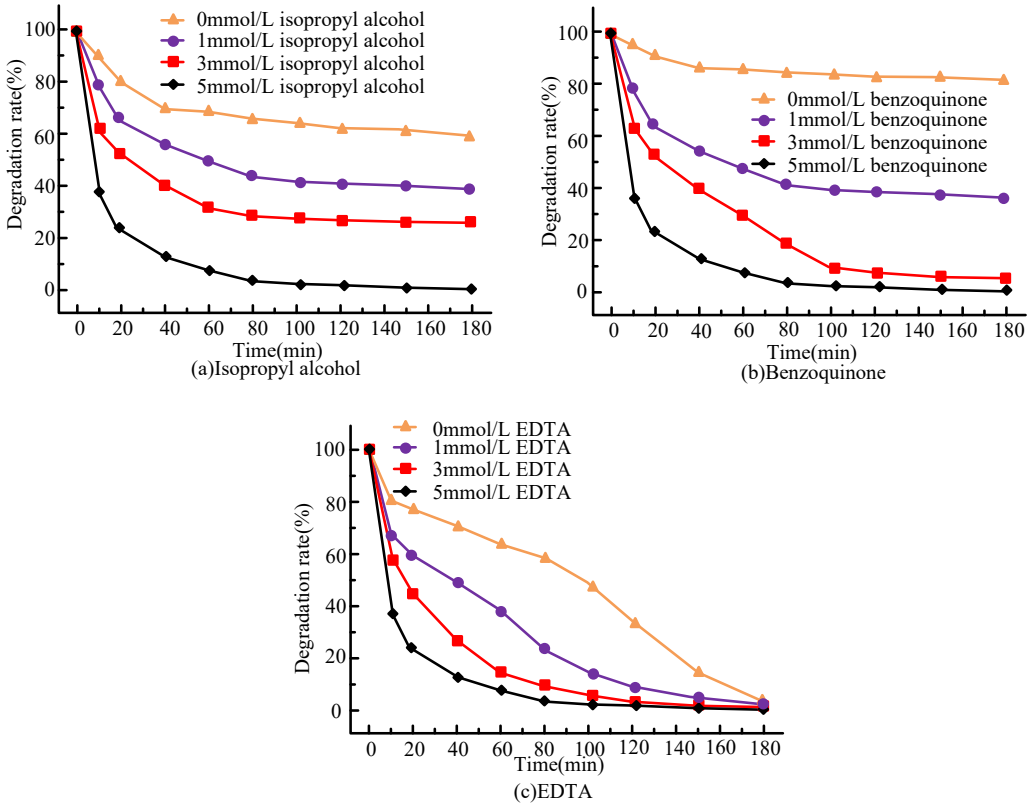

Figure 8. Under optimum conditions the capture agent (**a**) isopropyl alcohol, (**b**) p-benzoquinone, and (**c**) Effect of ethylenediaminetetraacetic acid on the degradation of bisphenol A by catalyst Fe3O4@B-rGO (9.3%).

As shown in Figure 8a, it can be seenthat the treatment rate of bisphenol A in the reaction system decreases with the increase in C_3H_8O concentration, and the ·OH maximum inhibition rate of the reaction system can reach 52.7%, indicating that ·OH is the most important active radical of the system. Figure 8b shows that the treatment efficiency of bisphenol A is significantly inhibited by p-benzoquinone, and the maximum inhibition rate of bisphenol A reached 71.2%. It shows that $O_2{\cdot}^-$ is also the main active free radical in this system. It can be seen from Figure 8c that the addition of EDTA did not significantly degrade the bisphenol A in the system, and its H^+ maximum inhibition rate is 6.8%. It can be seenthat the H^+ effect is not obvious in this system.

$O_2 \cdot^-$ in this reaction is discussed in relation to electron spin resonance spin trapping experiments, and the signal intensities of the corresponding ·OH radicals in the Fe_3O_4 and Fe_3O_4@rGO systems are compared. For the experimental results, see Figure 9.

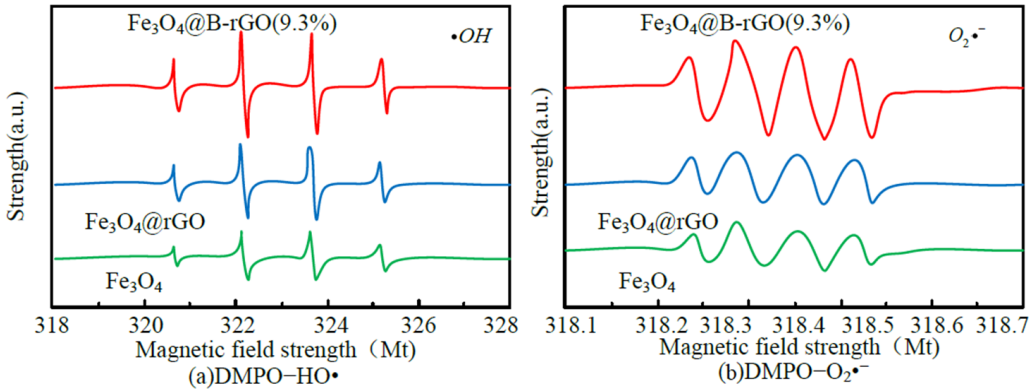

Figure 9. Electron spin resonance spectra of DMPO−HO• (**a**) and DMPO−O_2•$^-$ (**b**) adducts in visible-light Fenton system of different catalysts.

As shown in Figure 9, the spectrum contains DMPO-HO• characteristic peak with four times peak-to-peak ratio of 1:2:2:1 and DMPO-O_2•-typical signal peak with four times peak-to-peak ratio of 1:1:1:1, but the signal peak of the Fe_3O_4@B-rGO(9.3%) system is obviously stronger than the other two systems, indicating that in the Fe_3O_4@B-rGO(9.3%) system, the generation capacity of active free radicals ·OH and $O_2 \cdot^-$ is the highest among the three systems compared. Therefore, the heterogeneous Fenton photocatalytic performance of the reaction system using Fe_3O_4@B-rGO (9.3%) as catalyst is higher than that of the reaction system using Fe_3O_4 and Fe_3O_4@rGO as catalysts. The production of Fe^{2+} and the consumption of hydrogen peroxide in the photo-Fenton reaction of Fe_3O_4@B-rGO (9.3%), Fe_3O_4@rGO and Fe_3O_4 are investigated and analyzed, and the results are shown in Figure 10.

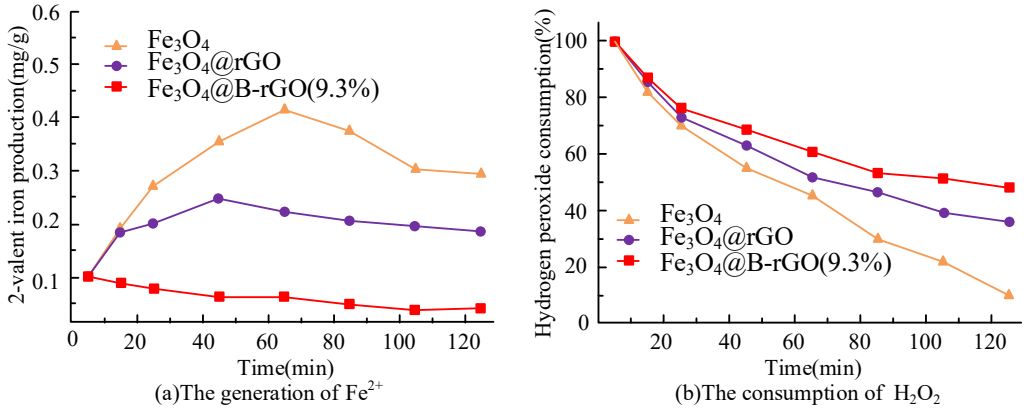

Figure 10. The generation of Fe^{2+} (**a**) and the consumption of hydrogen peroxide (**b**) during photo-Fenton.

It can be seen from Figure 10a that the Fe^{2+} in the catalyst Fe_3O_4 continues to decrease with the photo-Fenton reaction. For the catalysts Fe_3O_4@rGO and Fe_3O_4@B-rGO (9.3%), the production of Fe^{2+} increases first and then decreases. The catalyst Fe_3O_4@B-rGO (9.3%) has a higher Fe^{2+} production than the other two catalysts, which further proves that the photo generated electrons generated by B-rGO promote Fe^{2+} and Fe^{3+} cycles. It can be obtained from Figure 10b that the consumption of hydrogen peroxide by the catalyst Fe_3O_4 is 52.1% within 120 min. While for Fe_3O_4@rGO and Fe_3O_4@B-rGO (9.3%) systems, the consumption of hydrogen peroxide in time reached 63.9% and 90.5%, respectively.

5. Conclusions

Phenolic substances are contained in the wastewater discharged from many industrial and agricultural facilities. If these wastewaters are not treated, they will cause different pollution to the atmosphere, food, soil and water resources. The heterogeneous photo-Fenton catalyst Fe_3O_4@B-rGO was successfully prepared in the experiment. The catalyst was doped with boron atoms to increase the band gap of Fe_3O_4@rGO, thus inhibiting the recombination of photo-generated electrons and holes, and accelerating the transfer of photo-generated electrons from B-rGO to Fe_3O_4 to promote the conversion of Fe^{2+} to Fe^{3+} in the catalyst, thus increasing the heterogeneous photo-Fenton reaction rate. In addition, the catalyst has features of stable structure, good magnetism and easy recycling. Specifically, the catalyst has higher specific surface area and pore volume than nano-Fe_3O_4, which can provide more active centers for the reaction. In addition, the catalyst Fe_3O_4@B-rGO doped with different ratios of boron atoms showed good catalytic activity in the treatment of bisphenol A in the heterogeneous photo-Fenton system. Among them, Fe_3O_4@B-rGOwith a doping content of 9.3% is the most suitable catalyst for this system. The treatment efficiency of this catalyst to bisphenol A can reach 100% and the conversion rate is 67.4%. The research conclusion also confirms the generation of the main active radicals ·OH and $O_2\cdot^-$, and the catalyst Fe_3O_4@B-rGO (9.3%) can produce more active radicals than Fe_3O_4 and Fe_3O_4@rGO. From the specific data of the experimental results, it can be seen that although a similar method is adopted, the results of this study show that the catalyst prepared in this experiment has a higher reaction rate than the catalyst prepared in the reference, and can realize the complete degradation of pollutants, so its performance is better than that of the catalyst in the reference. It should be noted that due to the limited time, the research only focuses on whether doping boron atoms have an effect on the heterogeneous photo-Fenton catalytic activity. In the future study, the introduction of other atoms such as nitrogen atoms or sulfur atoms in related fields should also be studied.

Author Contributions: B.L. and X.Z. selected samples for test. Z.S. compared the experimental results. B.L. made further analysis. All authors conducted the experiments and analysed the results. All authors discussed the results and wrote the manuscript. All authors have read and agreed to the published version of the manuscript.

Funding: The research is supported by: Ningxia Natural Science Foundation in 2021 (2021AAC03174); Ningxia Natural Science Foundation in 2022 (2022AAC03282); The scientific research start-up project for recruitment talents of North Minzu University in 2021 (2021KYQD21); North Minzu University General Research Project in 2022 (2022XYZSK02, 2022XYZHG02).

Data Availability Statement: All data generated or analysed during this study are included in this published article.

Conflicts of Interest: The authors declare no conflict of interest.

References

1. Carvalho, N.; Chaim, O.; Cazarini, E.; Gerolamo, M. Manufacturing in the fourth industrial revolution: A positive prospect in sustainable manufacturing. *Procedia Manuf.* **2018**, *21*, 671–678. [CrossRef]
2. Horton, P.; Horton, B.P. Re-defining sustainability: Living in harmony with life on Earth. *One Earth* **2019**, *1*, 86–94. [CrossRef]
3. Padilla-Rivera, A.; Morgan-Sagastume, J.M.; Noyola, A.; Güereca, L.P. Addressing social aspects associated with wastewater treatment facilities. *Environ. Impact Assess. Rev.* **2016**, *57*, 101–113. [CrossRef]
4. Chowdhary, P.; Bharagava, R.N.; Mishra, S.; Khan, N. Role of industries in water scarcity and its adverse effects on environment and human health. In *Environmental Concerns and Sustainable Development*; Springer: Singapore, 2020; pp. 235–256.
5. Inyinbor Adejumoke, A.; Adebesin Babatunde, O.; Oluyori Abimbola, P.; Adelani Akande Tabitha, A.; Dada Adewumi, O.; Oreofe Toyin, A. Water pollution: Effects, prevention, and climatic impact. *Water Chall. Urban. World* **2018**, *33*, 33–47.
6. Said, K.A.M.; Ismail, A.F.; Karim, Z.A.; Abdullah, M.S.; Hafeez, A. A review of technologies for the phenolic compounds recovery and phenol removal from wastewater. *Process Saf. Environ. Prot.* **2021**, *151*, 257–289. [CrossRef]
7. Sawicka, B.; Skiba, D.; Umachandran, K.; Dickson, A. Alternative and new plants. In *Preparation of Phytopharmaceuticals for the Management of Disorders*; Academic Press: Cambridge, MA, USA, 2021; Volume 1, pp. 491–537.
8. Unuofin, J.O.; Odeniyi, O.A.; Momba, M.N.B. Algal biomass production coupled to wastewater treatment. In *An Integration of Phycoremediation Processes in Wastewater Treatment*; Elsevier: Amsterdam, The Netherlands, 2022; pp. 17–40.

9. Madhav, S.; Ahamad, A.; Singh, A.K.; Kushawaha, J.; Chauhan, J.S.; Sharma, S.; Singh, P. Water pollutants: Sources and impact on the environment and human health. In *Sensors in Water Pollutants Monitoring: Role of Material*; Springer: Singapore, 2020; pp. 43–62.
10. Jiao, W.; Luo, S.; He, Z.; Liu, Y. Applications of high gravity technologies for wastewater treatment: A review. *Chem. Eng. J.* **2017**, *313*, 912–927. [CrossRef]
11. Qian, X.; Ren, M.; Zhu, Y.; Yue, D.; Han, Y.; Jia, J.; Zhao, Y. Visible light assisted heterogeneous Fenton-like treatment of organic pollutant via α-FeOOH/mesoporous carbon composites. *Environ. Sci. Technol.* **2017**, *51*, 3993–4000. [CrossRef] [PubMed]
12. Garcia-Muñoz, P.; Fresno, F.; Lefevre, C.; Robert, D.; Keller, N. Synergy effect between photocatalysis and heterogeneous photo-Fenton catalysis on Ti-doped $LaFeO_3$ perovskite for high efficiency light-assisted water treatment. *Catal. Sci. Technol.* **2020**, *10*, 1299–1310. [CrossRef]
13. Zhu, Y.; Zhu, R.; Yan, L.; Fu, H.; Xi, Y.; Zhou, H.; Zhu, G.; Zhu, J.; He, H. Visible-light Ag/AgBr/ferrihydrite catalyst with enhanced heterogeneous photo-Fenton reactivity via electron transfer from Ag/AgBr to ferrihydrite. *Appl. Catal. B Environ.* **2018**, *239*, 280–289. [CrossRef]
14. Phan, T.T.N.; Nikoloski, A.N.; Bahri, P.A.; Li, D. Heterogeneous photo-Fenton treatment of organics using highly efficient Cu-doped $LaFeO_3$ under visible light. *J. Ind. Eng. Chem.* **2018**, *61*, 53–64. [CrossRef]
15. Chen, W.H.; Xiong, J.H.; Teng, X.; Mi, J.X.; Hu, Z.B.; Wang, H.; Chen, Z. A novel heterogeneous Co (II)-Fenton-like catalyst for efficient phototreatment by visible light over extended pH. *Sci. China Chem.* **2020**, *63*, 1825–1836. [CrossRef]
16. Kilic, M.Y.; Abdelraheem, W.H.; He, X.; Kestioglu, K.; Dionysiou, D.D. Photochemical treatment of tyrosol, a model phenolic compound present in olive mill wastewater, by hydroxyl and sulfate radical-based advanced oxidation processes (AOPs). *J. Hazard. Mater.* **2019**, *367*, 734–742. [CrossRef] [PubMed]
17. Guo, C.; Tan, Y.; Yang, S.; Qian, Y. Development of phenols recovery process with novel solvent methyl propyl ketone for extracting dihydric phenols from coal gasification wastewater. *J. Clean. Prod.* **2018**, *198*, 1632–1640. [CrossRef]
18. Liu, C.; Liu, Y.; Dang, Z.; Zeng, S.; Li, C. Enhancement of heterogeneous photo-Fenton performance of core-shell structured boron-doped reduced graphene oxide wrapped magnetical Fe_3O_4 nanoparticles: Fe (II)/Fe (III) redox and mechanism. *Appl. Surf. Sci.* **2021**, *1*, 148886. [CrossRef]
19. Abou-Taleb, E.M.; Hellal, M.S.; Kamal, K.H. Electro-oxidation of phenol in petroleum wastewater using a novel pilot-scale electrochemical cell with graphite and stainless-steel electrodes. *Water Environ. J.* **2021**, *35*, 259–268. [CrossRef]
20. Kadhum, S.T.; Alkindi, G.Y.; Albayati, T.M. Remediation of phenolic wastewater implementing nano zerovalent iron as a granular third electrode in an electrochemical reactor. *Int. J. Environ. Sci. Technol.* **2022**, *19*, 1383–1392. [CrossRef]